THE PENNSYLVANIA STATE UNIVERSITY
SCHREYER HONORS COLLEGE

DEPARTMENT OF CHEMICAL ENGINEERING

RAPID AUTOMATED OPTIMIZATION OF RIBOSWITCH FUNCTION FOR SYNTHETIC BIOLOGY

WALKER HUSO
SPRING 2015

A thesis
submitted in partial fulfillment
of the requirements
for a baccalaureate degree
in Chemical Engineering
with honors in Chemical Engineering

Reviewed and approved* by the following:

Howard Salis
Assistant Professor of Chemical Engineering
& Assistant Professor of Agricultural and Biological Engineering
Thesis Supervisor

Ali Borhan
Professor of Chemical Engineering
Honors Advisor

* Signatures are on file in the Schreyer Honors College.

ABSTRACT

Riboswitches are ligand dependent regulatory RNA's that can sense a specific ligand in the cellular environment and mediate a specific gene expression response to the detected ligand. Although significant progress has been made in identifying a variety of riboswitches that are directly coupled to activation, it is not clear how riboswitch sequences near the ligand binding site control the physics of riboswitch switching and translational activation. A better understanding of the biophysical principles governing switching would support the rational design of novel riboswitches for synthetic biology and could have transformative applications in remediating the environment, providing new medical therapies and diagnostics, or in developing new sensitive biosensors. We developed a biophysical model and an automated design method to convert aptamers into functional riboswitches. To validate our approach, we utilized 7 different aptamers to design and characterize 62 novel synthetic riboswitches with highly divergent sequences and structures. We validated predicted function with actual function. As part of this effort, we describe the design and characterization of riboswitches with specificity for dinitrotoluene (DNT). We compared the effects of sequence optimization before and after the aptamer domain for the DNT ligand and characterized the activation ratios of DNT riboswitch variants using a red fluorescent protein reporter. By comparing activation of DNT riboswitch variants and the activation of other riboswitch variants, a biophysical model was validated that explains the basis for novel riboswitch functional optimization. Finally, a predictive online tool was created that can rapidly optimize sequences of any individual riboswitch and can automatically incorporate functional activity considerations into riboswitch design.

TABLE OF CONTENTS

LIST OF FIGURES

LIST OF TABLES

ACKNOWLEDGEMENTS

First of all, my sincere thanks to my mentor Dr. Howard Salis for his expert guidance and generosity in helping me complete this thesis project. I am also grateful to Dr. Ali Borhan for reading my thesis and Amin Borujeni from Dr. Salis's lab for going above and beyond in helping me and encouraging me in the lab. Thank you to everyone else in Dr. Salis's lab for making my time in the lab enjoyable and thank you to the Schreyer Honors College for their support.

Chapter 1

Introduction

An important premise in synthetic biology is that an engineering perspective can be used to insert new “operating systems” into cells to make wholesale changes and drive totally new functions for organisms much as software operating systems drive advances in technology applications for a variety of hardware systems (1-3). Riboswitches are small structured RNA switches which contain sensor and responder domains making them attractive as synthetic regulators that can deliver a designed change in gene expression in response to practically any small molecule ligand that is sensed (4). As our understanding of the details of the genome and riboswitch biological systems improve, opportunities are emerging to develop riboswitch-based innovative solutions to long-standing problems in fields as diverse as medical diagnostics and therapeutics, environmental remediation, and materials production (5,6). The ability to rapidly design and predict functional activity of synthetic riboswitches would provide important advancements for the field of synthetic biology (7).

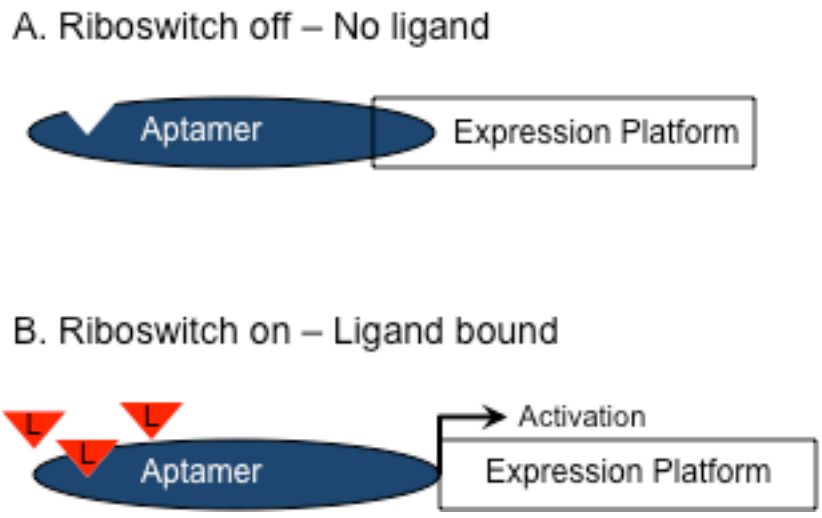

Figure 1. Riboswitch architecture and ligand mediated control of gene expression. **A.** In the absence of ligand, the pseudoknot structure of the riboswitch keeps it "off" and for example, obstructing access for ribosome-mediated translation. **B.** In the presence of ligand (L), the ligand binds specifically to the aptamer site turning the riboswitch "on" and for example, allowing access for ribosomal-mediated translation and activation of the gene expression platform.

Riboswitches

Riboswitches were first discovered over a decade ago as sensors and vitamin derivatives that control gene expression in bacteria (8-10). Riboswitches have been most extensively characterized in prokaryotes where they function as direct sensors of cellular metabolites, ions and proteins (11,12). However, they have also been shown to regulate gene expression in eukaryotes and a recent study has suggested the presence of adenosine binding RNA based aptamers in vertebrate genomes (13, 14). In general, when metabolite abundance exceeds a threshold level, the metabolite binds to a specific riboswitch sensor domain and induces a conformational change in the RNA expression platform domain which modulates downstream gene expression events (15,16, and Figure 1). Riboswitches are genetic circuits unique in their ability to bind diverse small ligands with their aptamer sensor domains without any requirement

for intermediate molecules (6). Riboswitches occur either as natural riboswitches that function in a variety of cells or as synthetic riboswitches which are forward engineered in the laboratory to serve a specific purpose (17-19).

Natural Riboswitches

Natural riboswitches are regulatory segments of mRNA that bind with specificity to a small molecule such as a metabolite, resulting in a change in the production of proteins encoded by the mRNA. Natural riboswitches can, for example, control translation, ribozyme activity, transcription, and mRNA splicing (20,21). They occur in a variety of organisms including bacteria, yeast, plants, and eukaryotes (22). In eukaryotes, the presence of introns and the fact that transcription and translation are uncoupled, necessitate different mechanisms to regulate gene expression by riboswitches. In this setting, eukaryotic TPP riboswitches regulate genes via alternative splicing—a process in which introns are excised and exons rejoined in different combinations to yield alternatively spliced mRNAs rather than riboswitches that target translation and/or transcription (23). In most cases, riboswitches act in cis as part of the RNA transcript, but they can also act in trans like an RNA binding protein (24,25), as an sRNA-like terminated riboswitch (26), or as an antisense RNA (27). Experimentally validated, naturally occurring riboswitches include those with specificity to purine (28), metal ions (29), fluoride (30), vitamin B12 (31), riboflavin (32), lysine (33), glycine (34), glutamine thiamine pyrophosphate (TPP) (23), and cyclic di-GMP (35) as well as others (Table 1). Although much has been learned about riboswitches over the past 10 years, there is still much that is unknown. Using genomics and bioinformatics, orphan riboswitches lacking a known ligand, are 2 of the 10

most commonly occurring riboswitches in genomes (36,37). In addition, it is predicted that there are hundreds of new classes of natural riboswitches yet to be discovered and will emerge as less common bacteria and other organisms have their genomes sequenced. (38)

Table 1. Examples of functional riboswitch targets.*

Coenzymes	Nucleotide derivatives	Amino Acids	Sugars	Ions	Small molecules
Vit B12	Guanine	Glycine	GlcN6P	Mg^{2+}	DNT
TPP	Adenine	Lysine		Ni^{2+}	Fluorine
FMN	PreQ1	Glutamine		Co^{2+}	FPP
THF	2'-dG				Theophylline
SAM	* c-di-GMP				Tetramethylrosamine
SAH					Dopamine
MoCo					Purine
Wco					Thyroxine

*Abbreviations: Vit B12 = cobamamide, TPP = thiamine pyrophosphate, FMN = flavin mononucleotide, THF = tetrahydrofolate, SAM = S-adenosyl methionine, SAH = S-adenosylhomocysteine, MoCo = molybdenum cofactor, Wco = tungsten cofactor, PreQ1 = pre-queuosine$_1$, 2'-dG = 2-deoxy-D-glucose, c-di-GMP = cyclic di-guanilate, GlcN6P = glucosamine-6-phosphate, Mg = magnesium, Ni = nickel, Co = cobalt, DNT = dinitrotoluene, FPP = farnesyl pyrophosphate

Synthetic Biology

In synthetic biology, switches have recently been used successfully in combination with other components, such as enzymes to assemble rationally designed metabolic pathways that produce biofuels (40) and therapeutic drugs (41), enable designer cells that potentially could correct metabolic diseases (42,43,44) and to develop novel biosensors (45). In spite of these successes, an underlying problem in synthetic biology remains the limited number of synthetic, high function parts for constructing genetic circuits along with difficulties that arise in developing large, complex synthetic networks from these limited parts (45).

Unlike electronic circuit elements, which can be electrically and spatially insulated from each other, biological components can interact with one another in the complex cellular environment and suffer from unwanted crosstalk between components. Overcrowding can also affect function inside living cells. Limitations imposed by the difficulties in developing synthetic biological circuit components, (e.g. synthetic riboswitches) hinder the construction of more complex, regulatable circuits that operate robustly in living cells without crosstalk interference. Consequently, new classes of synthetic regulated switches that offer low system crosstalk, computer-aided optimization, and high level functionality represent a much-needed, enabling step toward fully realizing the potential of synthetic biology in broad areas of biotechnology, bioengineering, and medicine (46).

Synthetic Riboswitches

RNA-based synthetic regulatory riboswitch elements offer a potential solution to this component bottleneck. Biological parts constructed from RNA take advantage of predictable Watson-Crick base pairing to predict responses and regulate cellular behavior. They are amenable to use of software tools for predicting RNA-RNA or RNA-ligand interactions as well as overall functionality. In addition, nature has already developed a wide assortment of natural RNA-based riboswitches that operate at the transcriptional and posttranscriptional levels of gene expression regulation and can be used to guide synthetic riboswitch development (5). Starting from these natural riboswitch systems, researchers have co-opted a number of functional regulatory switches that control translation and transcription in response to cognate ligands (47-53).

Aptamers

The sensor domain of a synthetic riboswitch offers great design flexibility and specificity since it is composed of a ligand-binding aptamer (6). Aptamers are short sequences of RNA that fold into specific 2D structures and bind with high affinity and specificity to target ligands through shape complementarity at the aptamer-target interface. (54) Aptamers can be synthesized and selected for the target of interest *in vitro* using a process termed systematic evolution of ligands by exponential enrichment (SELEX) (55,56). Aptamers of high affinity and specificity are selected from a large pool of ~10^{14} random oligonucleotides by sequential rounds of binding to target, removal of unbound oligonucleotides, and PCR amplification of bound aptamers. At the end of selection rounds, the highly enriched and reduced aptamer pool is subjected to cloning or sequencing followed by further characterization of individual aptamers. The advantages of SELEX are exemplified by the opportunity to select a high affinity, high specificity oligonucleotide aptamer to almost any ligand including inorganic or organic molecules, any protein, any cell, or even, for example, any organ of interest (57).

Biophysical Model of Riboswitch Design

Our biophysical model considers the riboswitch as an mRNA whose translation or output protein expression level is controlled by 1) interactions with its cognate ligand through its aptamer domain, and 2) interactions with the ribosome at its ribosome binding site. In the absence of ligand, the riboswitch folds into its minimum free energy state obscuring the Shine-Dalgarno sequence (ribosome binding site, RBS), binding only weakly to the ribosome (free energy $\Delta G_{total,OFF}$) and hampering the translation of the output protein. With ligand present, the

aptamer folds into a new minimum free energy state, exposing the Shine-Dalgarno sequence (free energy $\Delta G_{total,ON}$) and recruiting the ribosome for translation. The pre- and post- aptamer sequences are specifically designed to maximize the advantage of these states to promote effective riboswitch switching (57).

The activation ratio (AR) for each riboswitch can be represented by the formula $AR_{max} = \exp(-\beta [\Delta G_{total,ON} - \Delta G_{total,OFF}])$ indicating the maximum increase in the mRNA's translation initiation rate as determined by the difference in the ribosome's binding free energy at equilibrium and in the presence of excess ligand conditions (57). (Note: $\beta = 1/RT$ coefficient measured to be 0.45 mol/kcal for bacterial species) AR_{max} for any given riboswitch is calculated using the ribosome binding free energy model of the RBS Calculator v2.0 (59,60,61).

Several interactions contribute to the ribosome binding free energy for each riboswitch including: 1) the energy needed to unfold mRNA structures in its initial state that overlap with the ribosome footprint; 2) the energy released when ribosome 16S rRNA binds to the riboswitch mRNA; 3) the energy released when the initiator $tRNA^{fMet}$ base pairs to the start codon; 4) an energy penalty determined by the length of the spacer region that causes ribosomal stretching or compression; and 5) an energy penalty determined by the standby site's interactions with the ribosome's platform domain. These free energies for each riboswitch are summed to determine free energy $\Delta G_{total,OFF}$ for the ligand free state and free energy $\Delta G_{total,ON}$ for the ligand bound state. (58,62)

All parameters for the biophysical model were determined by previous measures of translation rates of mRNA's without aptamer domains (60,61). Base pairing energies were calculated by combining RNA free energy models that account for both secondary structures (63) and pseudoknots (64,65). Model calculations used two ingredients specific to each aptamer:

1) the aptamer domain structure when bound to its cognate ligand, and 2) the ligand's binding free energy. These parameters are known for hundreds of aptamers (66,67).

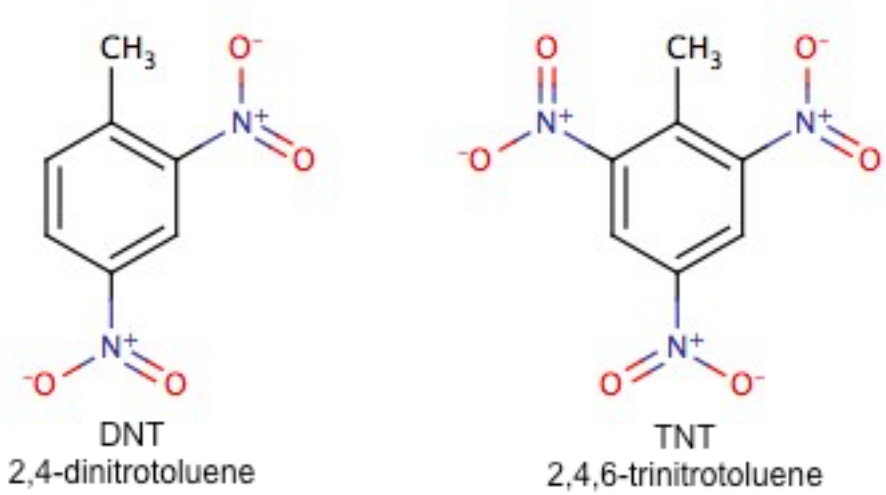

Figure 2. Comparison of DNT and TNT Structure. DNT is an important precursor in the synthesis of TNT. They are both cyclic aromatic hydrocarbons with either 2 or 3 nitro-groups. DNT is a stable, similarly detected, and closely related analog of TNT and is often used for laboratory studies to model TNT.

DNT as a Model Riboswitch

Trinitrotoluene (TNT) is the most widely used explosive worldwide. Dintrotoluene (DNT) is another dinitroaromatic compound that is closely related to TNT structurally, (Figure 2) less reactive, widely used to model TNT in the laboratory, and is a precursor in TNT synthesis (68,69). TNT poses significant health risks through contaminated soil or water in areas close to manufacturing or storage facilities or following militarization of particular areas. Metabolism of TNT in the human body produces cancerous derivatives (70). Therefore, there is an urgent need to develop sensors for fast, reliable, and inexpensive detection of explosives in soil, water, blood, urine or at airports (71). A synthetic DNT riboswitch offers a potential tool to address this need

for detection of trace amounts of dinitroaromatic compounds in a sensitive, specific and inexpensive way (72).

Significance

Although SELEX has provided a facile means to generate aptamers that bind to almost any relevant target, it remains difficult to engineer novel riboswitches that utilize the aptamers to detect and respond to ligands of interest. Most aptamers have therefore not been converted into robust, functioning riboswitches. For our studies, we used the DNT aptamer as a model to optimize riboswitch function in the detection of DNT. Comparing its optimization to other riboswitches we designed and optimized allowed us to gain a better understanding of how sequences around the ligand binding site control the biophysics of riboswitch switching. We developed a set of biophysical principles which govern the dynamics of activation for any synthetic riboswitch. We experimentally tested our approach by validating our model's predictions in riboswitches specific for DNT and a diverse variety of other ligands. Previously, we developed a model of ribosome-RNA interactions that predicts an mRNA's translation rate from its sequence. (52, 72) We used the new biophysical model to create an automated online tool to predict sequences needed that optimize riboswitch function for any aptamer based on sequence, the Riboswitch Calculator.

Chapter 2

Materials and Methods

DNT Riboswitches

DNT riboswitches were constructed and inserted into an mRFP1 fluorescent protein expression vector, derived from plasmid pFTV1 (ColE1 origin, CmR), using standard molecular cloning. Briefly, DNA fragments were computationally designed, synthesized, and assembled using either annealing of oligonucleotides, PCR assembly of oligonucleotides, or PCR amplification of gBLOCK DNA fragments (Integrated DNA Technologies). DNA fragments were then digested by XbaI and SacI restriction enzymes, followed by ligation with digested plasmid, transformation, plating on selective media, and verification of purified plasmid by sequencing. Similarly, promoter replacements were performed by annealing designed pairs of oligonucleotides, followed by digestion with BamHI/XbaI restriction enzymes, ligation, transformation, selective plating, and verification by sequencing.

The promoter AEB-3 was selected or designed to significantly vary riboswitch transcription rates (Supplementary Figure 12). The promoter AEB-3 is a result of mutating the -10 and -35 hexamers of J23100, resulting in 10-fold lower transcription rate. All DNT riboswitches used the AEB-3 promoter. The promoter sequences with underlined restriction sites are:

J23100 promoter: 5'-**GGATCC**GTTGACGGCTAGCTCAGTCCTAGGTACAGTGCTAGCT**TCTAGA**-3'

AEB-3 promoter: 5'-**GGATCC**TTGACAGCTAGCTCAGTCCTAGGGACTATGCTAGC**TCTAGA**-3'

Pre and Post-aptamer Sequences

Pre and post aptamer sequences were designed using a python computer code based on a statistical thermodynamic aptamer model. This code was run several times to find best the riboswitch sequences for characterization. The computer program generates 25 final pre and post aptamer sequences pairs each time it is run. In order to obtain these sequences the computer model rapidly iterates through a selectable number of generations modifying and characterizing the generated sequences as it goes. Finally the best sequences are selected and outputted when the program is finished. In our experiment we used 8 cores to process the computer code. With this set up each run was clocked at around 3000 seconds.

Ligand, Media, and Buffer Conditions

2,4- Dinitrotoluene (DNT) and DMSO were purchased from Sigma- Aldrich. Luria broth Miller (LB) media was purchased from VWR. DNT has a solubility of 1.48 mM (270 μg/mL) in water. To increase DNT solubility, 1% (v/v) DMSO was added to the media when characterizing DNT riboswitches and no-aptamer controls using the 0 mM DNT and 1 mM DNT conditions.

Growth, Fluorescence, and Luminescence Measurements

All fluorescence measurements were carried out using the strain E. coli DH10B during long-time cultures that maintain cells in the exponential growth phase. Cells harboring cloned plasmids expressing the mRFP1 reporter were grown overnight in 700 μl LB media and 50 μg/ml Cm antibiotic in a 96 deep-well plate at 370C and 200 rpm orbital shaking. Cultures were then

diluted to an OD600 of 0.01 into 200 µl LB media, 50 ug/ml Cm, and pre-defined concentrations of ligand and buffer solution. OD600 and fluorescence values were recorded by a M1000 spectrophotometer (TECAN) every 10 min until the OD600 reached about 0.15. Cells were then diluted to 0.01 into fresh media with the same composition, and grown until reaching mid-exponential phase. A third dilution was carried out in the same way. Time course fluorescence measurements per cell (FLPC) were analyzed by evaluating the equation

FLPC= F-FM - FNC -FM (3) OD600 -OD600,M OD600,NC -OD600,M

where F is the fluorescence of cells, FM is the fluorescence of media, FNC is the auto-fluorescence of non-transformed cells, OD600 is the optical density of cells, and OD600,M is the optical density of media.

Single-cell fluorescence levels were recorded by a Fortessa flow cytometer (BD Biosciences) and used to calculate activation ratios. During growth, and before each dilution, 10 µL samples were taken and added to 200 µL PBS with 2 mM kanamycin antibiotic for measurement. All distributions were unimodal. Auto-fluorescences of non-transformed cells were subtracted. Averages and standard deviations calculated from at least two independent measurements.

The addition of DNT to the media non-specifically increased reporter expression. The activation ratio for the no-aptamer control was 4.82-fold. In our data analysis, we eliminated the effects of non-specific expression changes by dividing the raw activation ratio determined for each DNT riboswitch by the activation ratio of the no-aptamer control (4.82) to yield the riboswitch-specific activation ratio which we report.

Materials

The dinitrotoluene used for this experiment was obtained from Sigma-Aldrich.

Bacterial Strain

The bacterial strains used were DH10B *E. coli*.

Chapter 3

Experimental Results

A program of automated computational procedures based our biophysical model was developed that used least free energy folding calculations to integrate functional predictions into riboswitch design (58). A set of riboswitches with specificity for DNT were constructed that had optimized predicted function integrated into their design, to test our predictions in living cells. Our DNT riboswitch backbone was designed with an aptamer, pre- and post-aptamer sequences, and the mRFP reporter. First, an aptamer sequence with DNT specificity was chosen based on previous studies (68). Computationally designed 25 nt pre and post-aptamer sequences were added. After the post-aptamer sequence, we added sequence encoding an AUG start site and the mRFP reporter. Next, the complete riboswitch sequence was used to guide synthesis of gBlock fragments of DNA. Full-length sequence were derived and amplified from the gBlocks and restriction sites were added for cloning using synthesized oligonucleotide primers and PCR. The construct was cloned into the pFTV1 plasmid and transfected into *E. coli* for expression. Expression was assessed *in vivo* by quantification of mRFP expression with flow cytometry (Figure 3A).

Our biophysical model considers a riboswitch as a long mRNA whose interactions with its cognate ligand and ribosome control its translation rate and thereby its reporter protein's expression level. Folding of the riboswitch RNA is dictated by contact with ligand. The detailed predicted structure for the DNT aptamer was modeled as a 2D structure using Mfold and it's predicted bound form is shown (Figure 3B). The aptamer is 86 nt in length and has a unique

hairpin stem-loop structure that is predicted to facilitate access to the ribosome binding site in the presence of ligand. Thus, in the presence of ligand, the riboswitch is predicted to be activated and turns on translation of the reporter through improved access to the ribosome binding site (part of post-aptamer sequence) for the cellular translational machinery and leading to increased expression.

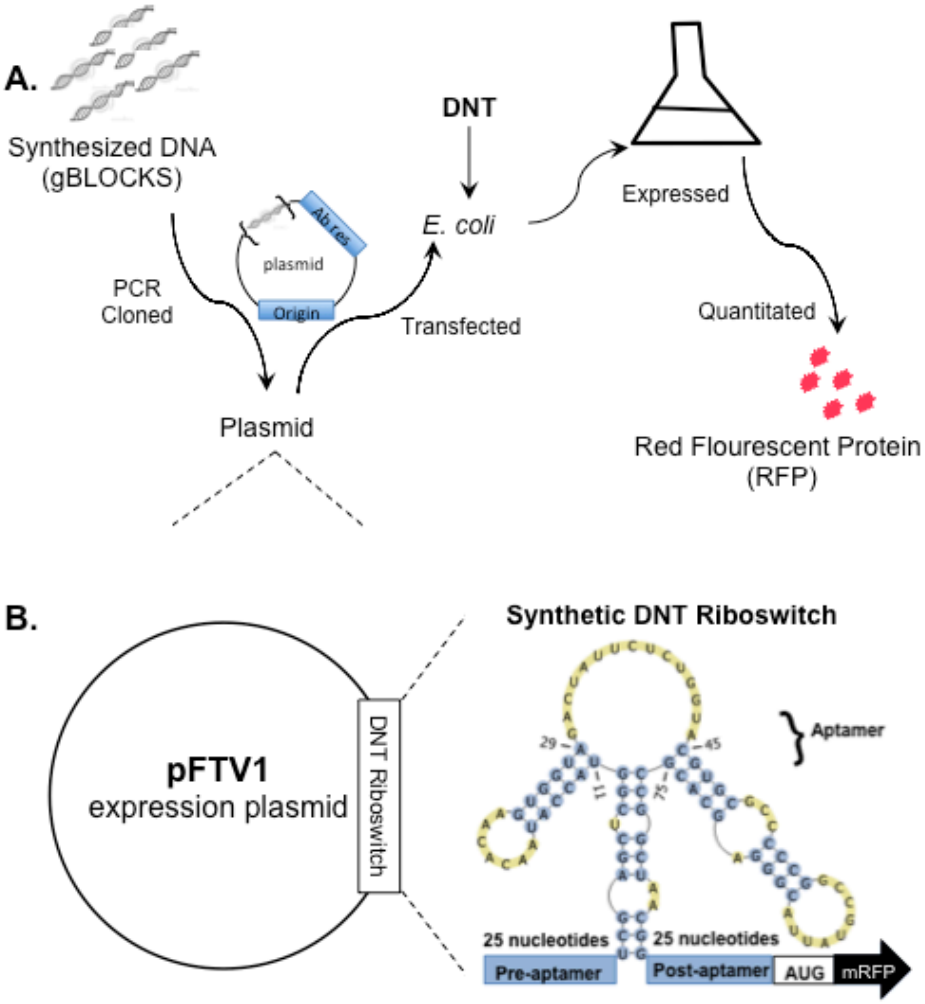

Figure 3. DNT riboswitch construct. A. A synthetic DNA riboswitch was synthesized, PCR cloned into the pFTV1 expression plasmid, transfected into *E. coli*, and assessed by measuring RFP expression in response to varying concentrations of DNT. **B.** The synthetic DNT riboswitch consists of pre-aptamer, aptamer, and post-aptamer sequences linked to Red Flourescent Protein (RFP). The aptamer sequence folds into a 2-dimensional structure (predicted structure as shown) which binds specifically to DNT triggering RFP expression.

The 25 nt pre-aptamer sequences were optimized for predicted riboswitch function based on our biophysical model. We chose the three optimized pre-aptamer sequences with the highest predicted function for experimental *in vivo* validation in the presence and absence of ligand in live cells. The 3 optimized pre-aptamer sequences are shown in Table 2 and designated as preDNT-6, preDNT-5, and preDNT-4. There were no differences in sequence in the first 6 nucleotides of the 3 pre-aptamer sequences. The preDNT-5 had 9 nucleotide differences from the preDNT-6 sequence across the 25nt that made up each. The preDNT-4 sequence had 9 nucleotide differences from preDNT-6 and 12 nucleotide differences from preDNT-5. (Table 2)

Table 2 Pre-aptamer sequence optimization for DNT aptamers

Aptamer I.D.	**Pre-aptmer sequence**
preDNT-6	**TCTAGAGTCGAAGATAAGGCCGCTT**
preDNT-5*	**TCTAGAGGCTAAATTAGCACTACTT**
preDNT-4**	**TCTAGAAGCTATTACAAGGGGCCT**
* = Differences from preDNT-6 sequence in red	
** = Differences from preDNT-6 sequence in red; from preDNT-5 sequence underlined	

The folded secondary structure of each of the 3 optimized 25nt pre-aptamers were predicted using Mfold. Each 25 nt sequence folded into similar short hairpin stem-loop structures with slight differences (Figure 4). Based on predictions for DNT-4 and DNT-6, 6 of 25 nt paired into non-branched stem structures and 19/25 nt formed two unpaired loop/bulge structures which were very similar to each other. DNT-5 secondary structure was characterized by 14 of 25 nt paired into non branched stem structures and 11 of 25 nucleotides comprised 3 small unpaired loop/bulge structures. The secondary structures were the least free energy folded structures and were predicted to be most likely formed in the presence of ligand.

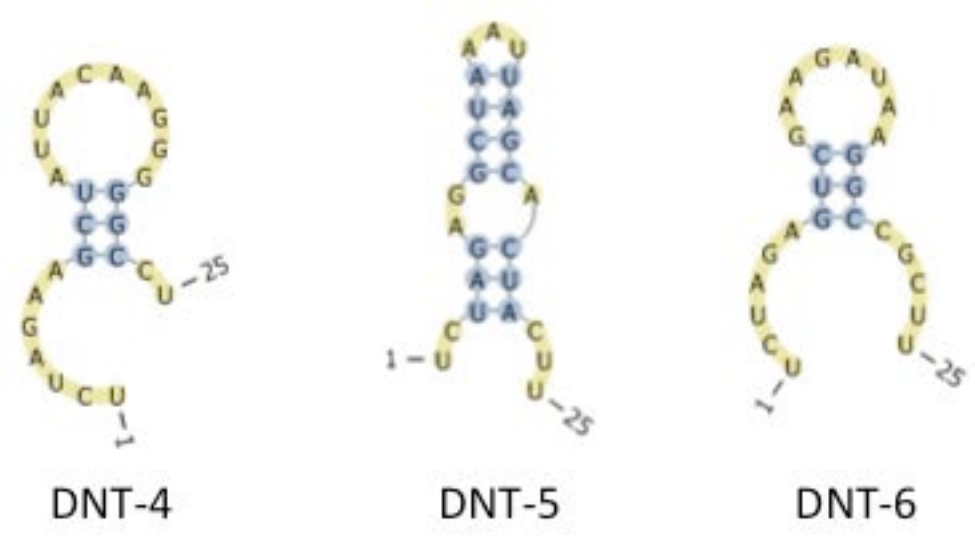

Figure 4. Pre-aptamer sequence folding. The 2D structre of the 25 pre-aptamer sequence. Structures obtained uisng Mfold. The most energetically favorable structure chosen for each.

The 25 nt post-aptamer sequences were also optimized for predicted riboswitch function based on our biophysical model. We chose the three optimized post-aptamer sequences which had the least free energy and highest predicted function for experimental *in vivo* validation in the presence and absence of ligand in live cells. The 3 optimized post-aptamer sequences are shown in Table 3 and designated as postDNT-6, postDNT-5, and postDNT-4. There was only one nucleotide difference in the 3 post-aptamer sequences across the final 12 of 25 nucleotides of the sequence and that was an A to T change at nt 23 in postDNT-4. Overall the postDNT-5 has 8 nucleotide differences from the postDNT-6 sequence across the 25nt that make up each. The postDNT-4 sequence had 10 nucleotide differences from postDNT-6 and 12 nucleotide differences from postDNT-5. (Table 3)

Table 3. Post-aptamer sequence optimization for DNT aptamer

Aptmaer I.D.	Post aptamer sequence
postDNT-6	**AATAAGCGCACCGAGGAGGTCAAAT**
postDNT-5*	**TCGTAGCACCTAGAGGAGGTCAAAT**
postDNT-4**	**AAGCTCTAGACTCAGGAGGTCATAT**
* = Differences from sequence postDNT-6 in red	
** = Differences from sequence post-DNT-6 in red; from postDNT-5 underlined	

In our construct, the full length sequence that follows the DNT aptamer included both the 25nt post-aptamer sequence and the reporter sequence, mRFP. We therefore used Mfold to predict the folded secondary structure of each of the 3 optimized full post-aptamer sequences including the 25nt post-aptamer sequence together with the mRFP reporter sequence for each of the 3 riboswitches (total 125 nt each). (Figure 5) Each 125 nt sequence was predicted to fold into similar extended hairpin stem-loop secondary structures with slight differences in each. For DNT-4, 70 of 125 nt paired into an extended hairpin stem structure with one short branch and 55 of 125 nt formed seven distinct unpaired nt loop/bulge structures. For DNT-6, 66 of 125 nt paired into an extended hairpin stem structure with a single short branch and 59 of 125 nt formed seven small loop/bulge structures of unpaired nt. For DNT-4, 60 of 125 nt paired into an extended hairpin stem structure with two short branches and 65 of 125 nt formed eight distinct unpaired nt loop/bulge structures. The secondary structures were the most likely lowest free energy structures for these sequences and were predicted to be most likely formed in the presence of ligand.

In the absence of ligand our prediction is that the riboswitch mRNA including the 25 nt pre-aptamer, the aptamer, the 25 nt post-aptamer and the sequence encoding mRFP, folds into a unique mRNA secondary structure. The least energy, folded secondary structure. for each full-

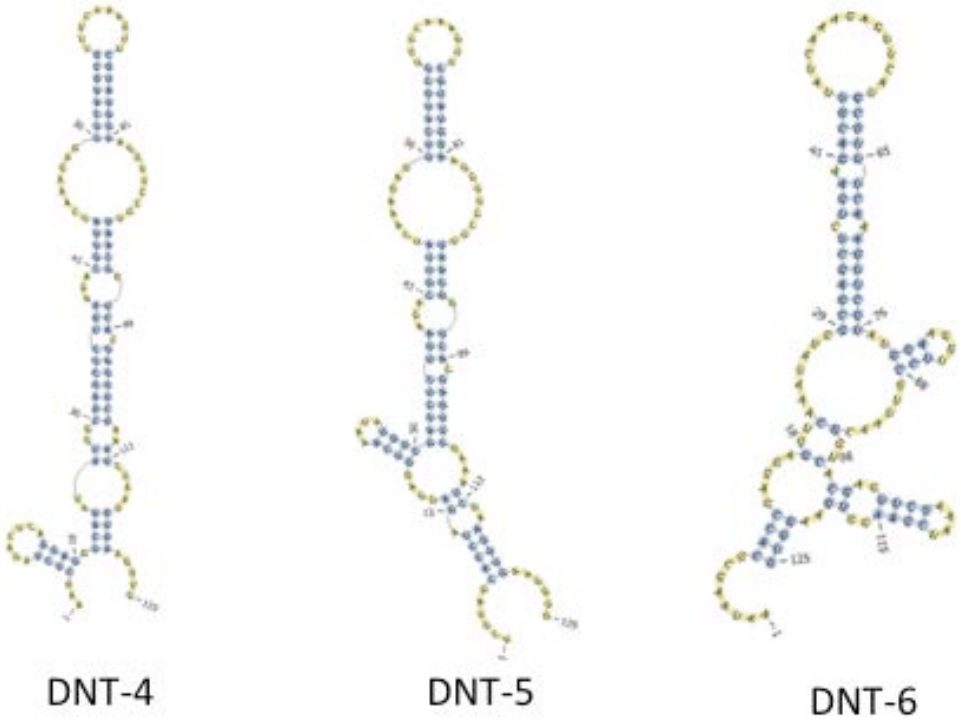

Figure 5. The 2D structure of the post-aptamer sequence including mRFP sequence. Structures obtained uisng Mfold. The most energetically favorable structure was chosen for each.

length riboswitch RNA was predicted using Mfold. for riboswitch DNT-4 (Figure 6), riboswitch DNT-5 (Figure 7), and riboswitch DNT-6 (Figure 8). Each folds into an extensively branched extended hairpin stem-loop structure 236 nt in length that is markedly different from the least energy secondary structures predicted for pre- and post-aptamer sequences in the presence of ligand (Figure 4, Figure 5). A black box outline was used to highlight the post-aptamer sequence in the absence of ligand (Figure 6,7,8) and demonstrated how the ribosome binding site in the post-aptamer sequence of each optimized DNT riboswitch may be inaccessible for the cellular translational machinery in the absence of ligand, leading to decreased expression.

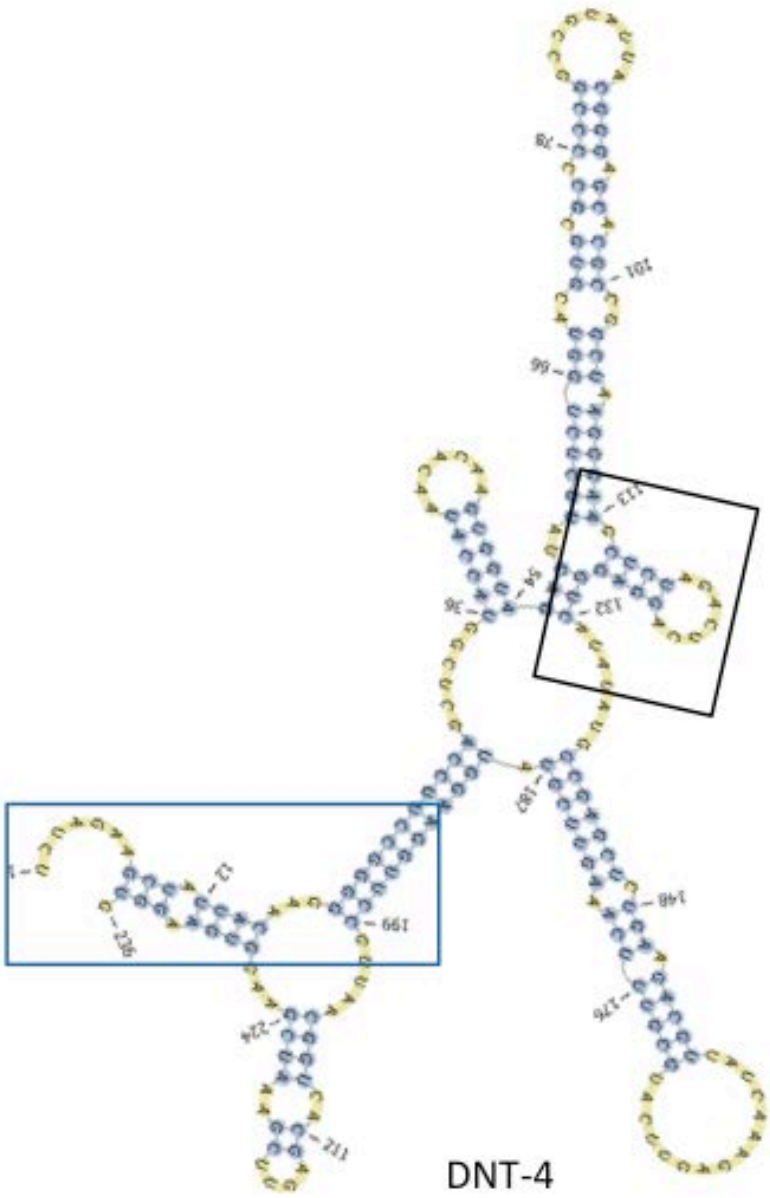

Figure 6. Structure, sequence, and folding of optimized DNT Riboswitches. The 2D structure of the full DNT-4 riboswitch. The predicted 2D structure of the pre-aptamer (blue box) and the post aptamer (black box) sequences are shown in the context of the full riboswitch., DNT aptamer, post-aptamer and RFP reporter sequences were modeled as shown using Mfold.

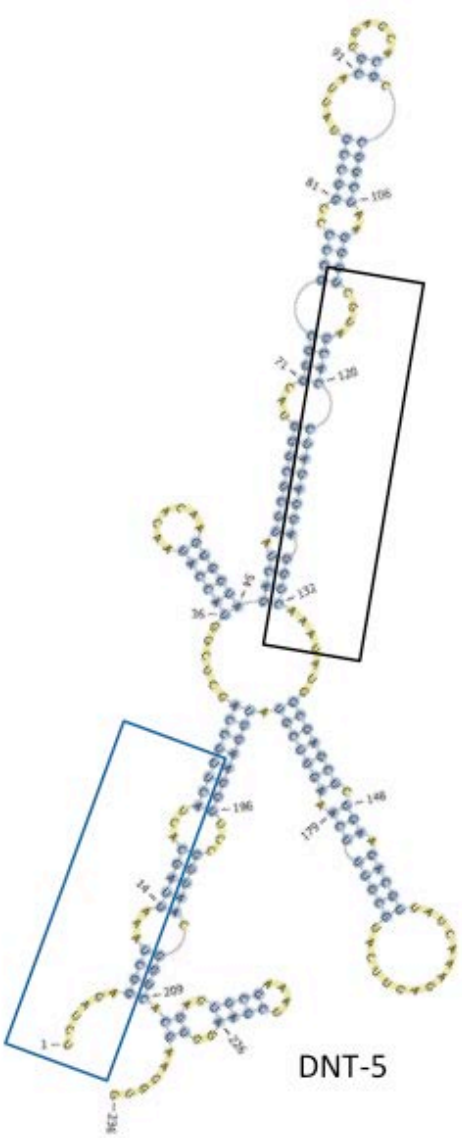

Figure 7. Structure, sequence, and folding of optimized DNT Riboswitches. The 2D structure of the full DNT-5 riboswitch. The predicted 2D structure of the pre-aptamer (blue box) and the post aptamer (black box) sequences are shown in the context of the full riboswitch., DNT aptamer, post-aptamer and RFP reporter sequences were modeled as shown using Mfold.

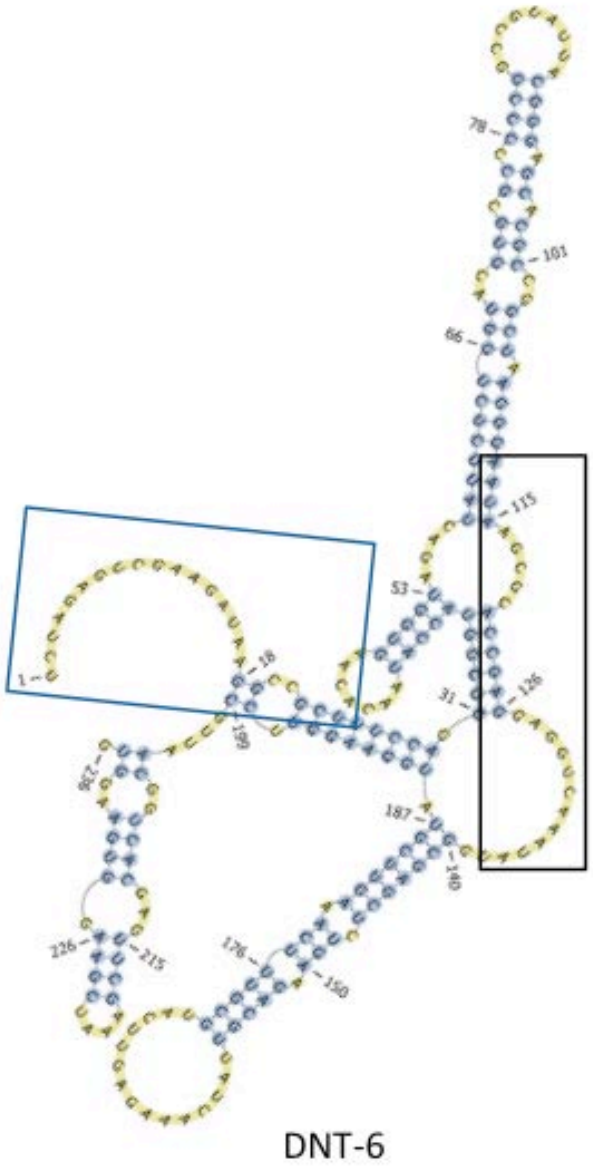

Figure 8. Structure, sequence, and folding of optimized DNT Riboswitches. The 2D structure of the full DNT-6 riboswitch. The predicted 2D structure of the pre-aptamer (blue box) and the post aptamer (black box) sequences are shown in the context of the full riboswitch., DNT aptamer, post-aptamer and RFP reporter sequences were modeled as shown using Mfold.

In order to validate our integration of riboswitch function considerations into the predictive design of the 3 optimized DNT riboswitches, we transfected each of the 3 cloned riboswitch constructs into *E. coli* and compared expression of the mRFP reporter in the absence

(0 mM) or presence (1 mM) of DNT (Figure 9). We measured mRFP by flow cytometry of the transfected cells. The DNT-4 riboswitch expressed ~10 au fluorescence in the absence of DNT while the DNT-5 riboswitch and the DNT-6 riboswitch expressed ~20 au fluorescence. In the presence of 1 mM DNT each riboswitch responded with activation of reporter expression, but to different levels. The DNT-4 riboswitch produced ~40 au fluorescence, DNT-5 riboswitch produced ~100 au fluorescence and the DNT-6 riboswitch produced ~140 au fluorescence in the presence of 1 mM DNT. Therefore each riboswitch exhibited low background expression in the absence of ligand and varying but high levels of riboswitch activation in response to the DNT ligand (Figure 9).

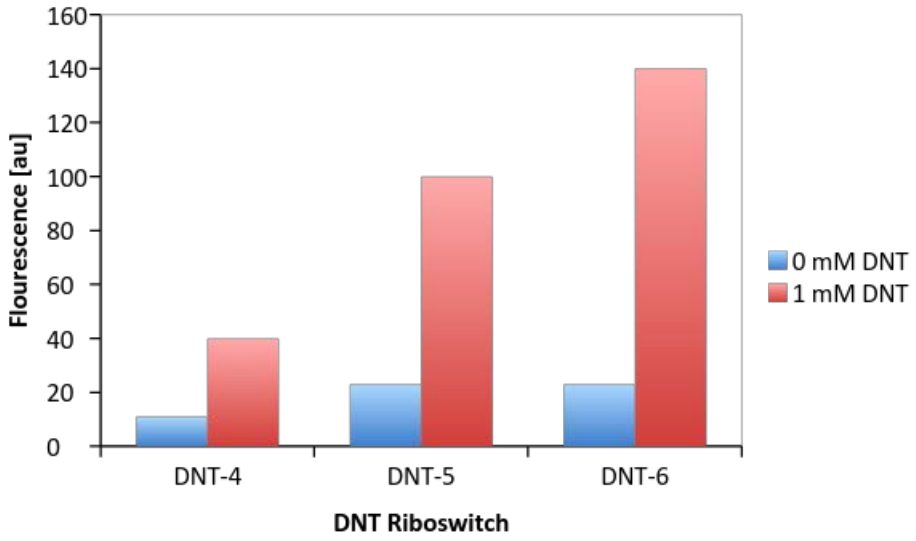

Figure 9. DNT riboswitch function *in vivo. E. coli* were transfected with the PFTv1 plasmid. Red fluorescent protein reporter expression was measured in the presence or absence of 1mM DNT in the media. RFP was measured using flow cytometry (RFP Emax of 551ex/594em; au= arbitrary units).

We next correlated the calculated least energy prediction value (ΔΔG) for each riboswitch with the corresponding predicted AR and validated AR for each DNT riboswitch. Validated AR

was calculated as (measured fluorescence in presence DNT)/(measured fluorescence in absence DNT). There was good correlation of the 3 indicators of riboswitch functional activity as the highest values for all 3 were associated with DNT-6 riboswitch while the lowest values for all 3 were associated with the DNT-4 riboswitch(Figure 10).

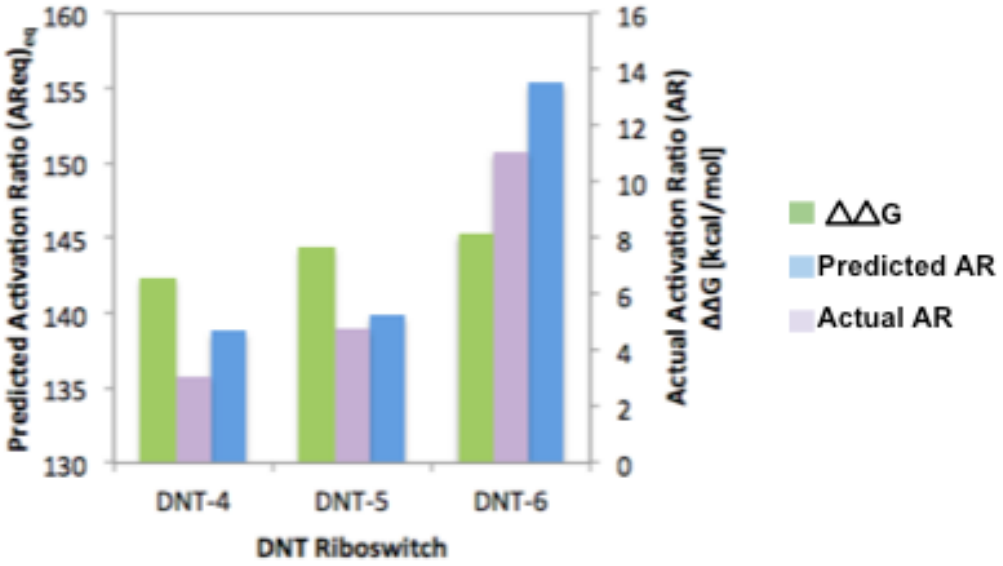

Figure 10. Comparing ΔΔG, Predicted AR, and Actual AR in DNT riboswitches. ΔΔG and predicted AR were predicted using the riboswitch calculator (see Fig. 11). Actual AR was determined experimentally by measuring *in vivo* activation of each DNT riboswitch (AR= activation [+DNT]/ activation [-DNT]).

In order to validate our riboswitch function predictions on a broader scale, we calculated the activation ratios from the 3 DNT riboswitches that we designed and optimized and found them to be: 1) 3 fold; 2) 4.5 fold; and 3) 11.1 fold activated in the presence of 1mM DNT ligand (Figure 11). We then compared the AR of the 3 DNT riboswitches with ARs for a varied set of 59 riboswitches that were designed in our lab with 6 different aptamer specificities, bringing the total to 62 riboswitch variants based on 7 different aptamer specificities. All of the riboswitches had varied levels of predicted optimized function based on our biophysical model and automated optimization. The aptamer specificities of the other riboswitches in addition to the DNT riboswitches were 1) theophylline, 2) alternate theophylline, 3) fluoride, 4) dopamine, 5) T4 (thyroxine) and 6) TMR (tetramethylrosamine). Overall, the measured riboswitch activation ratios varied from less than1 fold up to 383 fold for one of the theophylline riboswitch variants (Figure 11). These results suggest that the model can be used to successfully derive functional riboswitch variants engineered to detect non-ideal ligands.

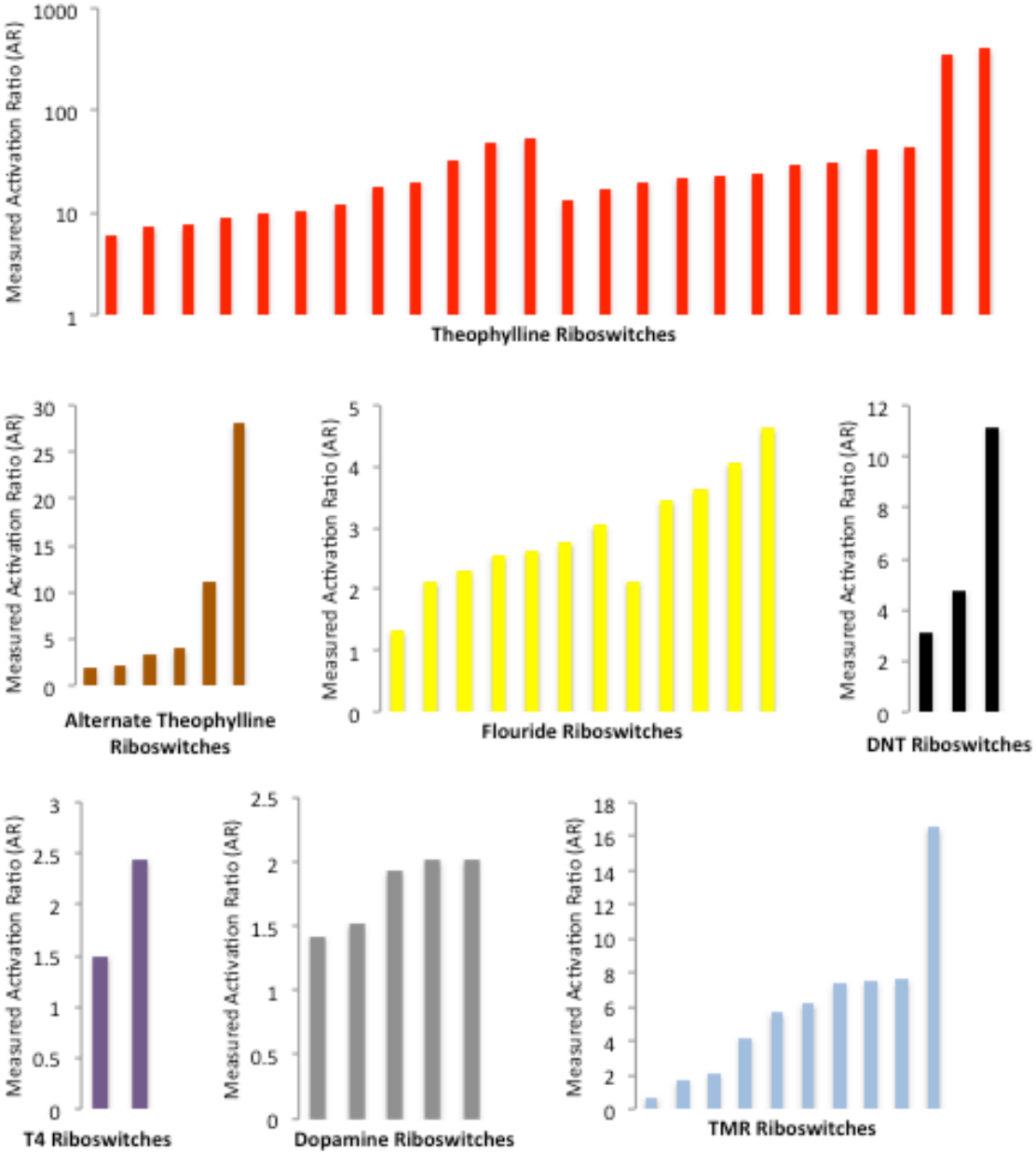

Figure 11. Comparison of functional activity (AR) in a variety of designed riboswitches. The activation ratio was determined for 62 riboswitches designed from 6 different aptamers by measuring reporter gene response in the presence and absence of each respective cognate ligand. (adapted from Borujeni, Huso, Salis submitted)

To gain a better understanding of the principles governing riboswitch function, we examined the correlation between the predicted and measured AR for DNT and the other riboswitches. We found that riboswitches with near-zero switching free energies had well-predicted activation ratios, but if switching free energy for the riboswitch was neglected, simply comparing AR of predicted and actual activation ratios was a poor predictor of riboswitch function. This was because as free energies grew, riboswitches became kinetically trapped and their activation ratios increasingly deviated from equilibrium calculations. When the ligand-bound state's instability was accounted for using our formula for AR_{actual} shown below,

$$AR_{actual} = 1 + \frac{\exp(-\beta(\Delta\Delta G_{mRNA} + \Delta G_{ligand}))}{1+\exp(-\beta(\Delta\Delta G_{mRNA} + \Delta G_{ligand}))} (AR_{eq}-1)$$

there was good agreement between model predictions and activation ratios for 120 measurements. The DNT riboswitch measurements were added to the figure (Figure 12) as examples of RNA aptamers with compelling applications, but lacking experimentally determined structures and well-measured binding affinities, unlike the other examples shown (Figure 12). The DNT riboswitches were measured in bacterial assays with an mRFP fluorescent reporter to measure each DNT riboswitch-specific activation ratio *in vivo*.

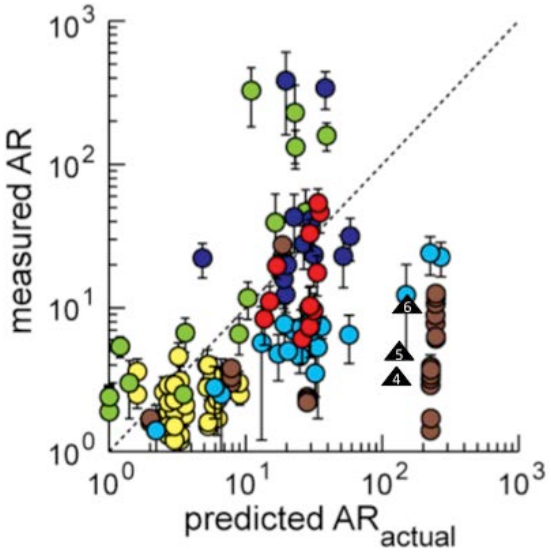

Figure 12. Agreement between Model predictions and measured activation ratios. Correlations are based on 120 measurements of the riboswitch activation ratios. DNT riboswitches 4, 5, and 6 are shown as black triangles. Other riboswitches are colored according to their aptamer: (dark blue) designed theophyline riboswitches; (red) theophyline riboswitches with mutated aptamer; (brown) theophyline riboswitches with different coding sequences; (green) previously engineered theophyline riboswitches; (yellow) designed flouride riboswitches; (light blue) TMR riboswitches (adapted from Bourujeni, Huso, Salis, et. al. submitted).

We next automated the calculations we used in developing our predictive biophysical model of riboswitch regulation into a free web-based interface that is easy to use and publicly available. We called this automated design method the Riboswitch Calculator. Automation of these calculations with the Riboswitch Calculator along with the availability of aptamers and their related design methods, enables the rapid prototyping of new biomolecular sensors and optimized functional riboswitches for a variety of purposes (Figure 13).

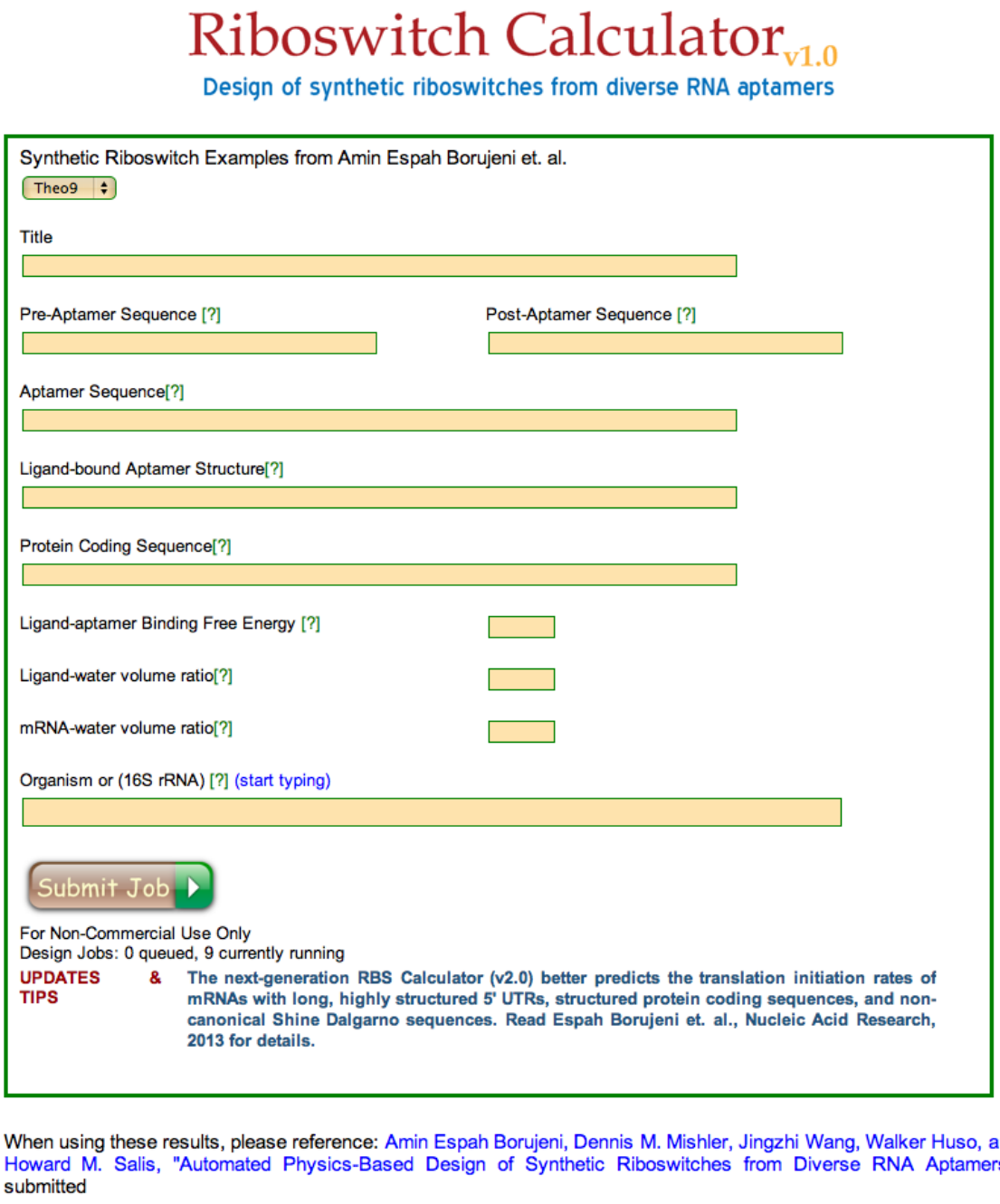

Figure 13. Home page of the Riboswitch Calulator: The online riboswitch calculator predicts the translation initiation rates of mRNAs with long highly structured 5' UTRs, structured protein coding sequences, and non-canonical Shine Delgarno sequences incorporating optimized function into the design of synthetic riboswitches. https://salis.psu.edu/software/RiboswitchCalculator_EvaluateMode

The automated design of novel synthetic riboswitches with predicted optimized function can be envisioned to follow a rational pathway that includes multiple steps (Figure 14). This new approach fills a void in RNA molecular design by replacing high throughput screening approaches with detailed physical chemistry calculations as a basis for improving riboswitch design predictions. The riboswitch calculator integrates these functional considerations into the design of novel riboswitches.

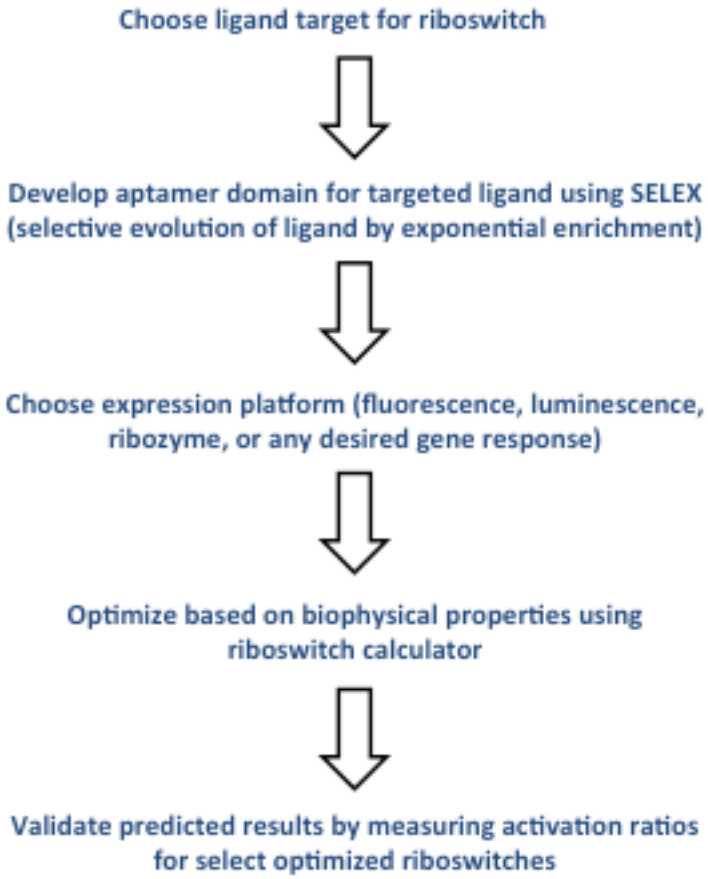

Figure 14. Schematic of successful design strategy for novel riboswitches for synthetic biology using computational biophysical model.

Chapter 4

Discussion and Future Directions

Our results describe the development of a set of riboswitches designed to respond to DNT. We used automated optimization to predict functional activity and validated the predictions in engineered cells designed to detect DNT and respond with a readily quantified mRFP fluorescent signal. More broadly, our results also address a challenge in designing RNA based molecular tools that has been long-standing and difficult. Our approach replaces tedious high throughput screening with detailed physical chemistry calculations and biophysical modeling. We developed a set of principles that govern riboswitch function and integrated functional predictions into automated riboswitch design. Our results demonstrate that careful selection of optimized pre- and post-aptamer sequences can have a profound effect on proper riboswitch function.

This is important because sensitive detection of nitro-aromatic explosives like DNT and TNT could have many applications in medicine and environmental contamination. In addition, exchanging the riboswitch expression platform domain from a fluorescent reporter to a DNT metabolizing output has the potential to move DNT riboswitch applications toward environmental remediation.

Furthermore our results provide a prototype strategy for optimization of any aptamer for function in the context of a riboswitch. Using riboswitches to build circuits for synthetic biology

has suffered from lack of a way to efficiently adapt high throughput results from aptamer screens into functional riboswitches. With the online riboswitch calculator we developed based on our modeling, that bottleneck has been alleviated by an automated process that appears to be highly relevant to developing functioning riboswitches from almost any aptamer-target pair that binds with high affinity. Pairing the riboswitch calculator with results from a SELEX screening approach should move the field of novel riboswitch design forward at a rapid pace.

Our hypothesis that pre- and post-aptamer sequences 25nt in length could provide a focus for functional optimization proved to be correct. We validated our predicted results using reporter expression platforms. We adjusted our predictions by incorporating considerations of variations in switching free energy in different aptamers and accounting for the ligand bound site instability producing good agreement between predicted and validated AR. Our findings built on our previous results and those of others, which focused in part on optimizing the ribosome binding site sequence for improving translational efficiency (59, 61). Insights gained in developing an automated calculator that optimizes ribosomal binding as well as our other calculators were important in helping to guide our current studies.

Our results raise further questions, which could be addressed in future studies. First, could this strategy for automated design based on biophysical modeling be applied to other methods of circuit building in synthetic biology? There are obvious advantages to having accurate and predictive automated calculators to assist in engineering genetic circuits. Additional automated calculators relevant to synthetic biology tools could be important in driving advances in the field. Second, How can the predictive accuracy of automated functional optimization be

improved? The prototype calculator, which we describe, provides a framework on which to build better and more predictive calculators of robust function in the future. Finally can DNT riboswitches move to more applied research settings and eventually meet the need for sensitive detection and safe remediation of problems associated with contamination by explosive materials. A web interface to the automated design method called the riboswitch calculator is accessible at salis.psu.edu/software.

In conclusion, integration of functional considerations into the design of DNT riboswitches was used to develop three new riboswitches which were specific for targeting DNT. We validated these for functional activity. The activation ratios of the three riboswitches varied from 3.2 to 11.1-fold activation as output was quantified with an mRFP reporter. DNT riboswitches hold considerable promise as an important tool in meeting the challenges of sensitive detection and remediation of DNT and related nitro-aromatic compounds whose use is widespread in the world today. Our studies provide a prototype strategy for optimizing riboswitches designed with almost any specificity.

Appendix A

Online Resources

1. https://salis.psu.edu/software/RiboswitchCalculator_EvaluateMode
2. http://mfold.rna.albany.edu/?q=mfold/RNA-Folding-Form
3. http://pseudoviewer.inha.ac.kr
4. https://salis.psu.edu/software/RBSLibraryCalculatorSearchMode
5. https://salis.psu.edu/software/forward
6. https://salis.psu.edu/software/SmallRNACalculator_ReverseEng
7. https://salis.psu.edu/software/OperonCalculator_EvaluateMode

BIBLIOGRAPHY

1. Annaluru N, Muller H, Mitchell LA, Ramalingam S, Stracquadanio G, Richardson SM, Dymond JS, Kuang Z, Scheifele LZ, Cooper EM, Cai Y, Zeller K, Agmon N, Han JS, Hadjithomas M, Tullman J, Caravelli K, Cirelli K, Guo Z, London V, Yeluru A, Murugan S, Kandavelou K, Agier N, Fischer G, Yang K, Martin JA, Bilgel M, Bohutski P, Boulier KM, Capaldo BJ, Chang J, Charoen K, Choi WJ, Deng P, DiCarlo JE, Doong J, Dunn J, Feinberg JI, Fernandez C, Floria CE, Gladowski D, Hadidi P, Ishizuka I, Jabbari J, Lau CY, Lee PA, Li S, Lin D, Linder ME, Ling J, Liu J, Liu J, London M, Ma H, Mao J, McDade JE, McMillan A, Moore AM, Oh WC, Ouyang Y, Patel R, Paul M, Paulsen LC, Qiu J, Rhee A, Rubashkin MG, Soh IY, Sotuyo NE, Srinivas V, Suarez A, Wong A, Wong R, Xie WR, Xu Y, Yu AT, Koszul R, Bader JS, Boeke JD, Chandrasegaran S. Total synthesis of a functional designer eukaryotic chromosome. 2014. Science. 344:55-58.

2. Gibson DG, Glass JI, Lartigue C, Noskov VN, Chuang RY, Algire MA, Benders GA, Montague MG, Ma L, Moodie MM, Merryman C, Vashee S, Krishnakumar R, Assad-Garcia N, Andrews-Pfannkoch C, Denisova EA, Young L, Qi ZQ, Segall-Shapiro TH, Calvey CH, Parmar PP, Hutchison CA 3rd, Smith HO, Venter JC. Creation of a bacterial cell controlled by a chemically synthesized genome. 2010. Science. 329:52-56.

3. Gibson DG, Venter JC. Synthetic biology: Construction of a yeast chromosome. 2014. Nature. 509:168-169.

4. Barrick JE, Corbino KA, Winkler WC, Nahvi A, Mandal M, Collins J, Lee M, Roth A, Sudarsan N, Jona I, Wickiser JK, Breaker RR. New RNA motifs suggest an expanded scope for riboswitches in bacterial genetic control. 2004. PNAS. 101:6421-6426.

5. Breaker RR, Joyce GF. The expanding view of RNA and DNA function. 2014. Chem Biol. 21:1059-1065.

6. Serganov A, Nudler E. A decade of riboswitches. 2013. Cell. 152:17-24.

7. Borujeni AE, Mishler DM, Wang J, Huso W, Gallivan JP, and Howard M. Salis HM. The Riboswitch Calculator: automated physics-based design of synthetic riboswitches from diverse RNA aptamers. Abstract. RNA Meeting, October 16-17, 2014. Pittsburg, PA.

8. Winkler WC, Cohen-Chalamish S, Breaker RR. An mRNA structure that controls gene expression by binding FMN. 2002. PNAS. 99:15908-15913.

9. Mironov AS, Gusarov I, Rafikov R, Lopez LE, Shatalin K, Kreneva RA, Perumov DA, Nudler E. Sensing small molecules by nascent RNA: a mechanism to control transcription in bacteria. 2002. Cell. 111:747-756.

10. Nahvi A, Sudarsan N, Ebert MS, Zou X, Brown KL, Breaker RR. Genetic control by a metabolite binding mRNA. 2002. Chem Biol. 9:1043.

11. Mellin JR, Koutero M, Dar D, Nahori MA, Sorek R, Cossart P. Riboswitches. Sequestration of a two-component response regulator by a riboswitch-regulated noncoding RNA. 2014. Science. 345:940-943.

12. Mellin JR, Cossart P. Unexpected versatility in bacterial riboswitches. 2015. Trends Genet. 31:150-156.

13. Perreault J, Weinberg Z, Roth A, Popescu O, Chartrand P, Ferbeyre G, Breaker RR Identification of hammerhead ribozymes in all domains of life reveals novel structural variations. 2011. PLoS Comput Biol. 7(5):e1002031.

14. Vu MMK, Jameson NE, Masuda SJ, Lin D, Larralde-Ridaura R, and Lupták A. Convergent evolution of adenosine aptamers spanning bacterial, human, and random sequences revealed by structure-based bioinformatics and genomic SELEX. 2012. Chem. Biol. 19:1247–1254.

15. Chen J, Gottesman S. RNA. Riboswitch regulates RNA. 2014. Science. 345:876-877.

16. Zhang J, Ferré-D'Amaré AR. Co-crystal structure of a T-box riboswitch stem I domain in complex with its cognate tRNA. 2013. Nature. 2013. 500:363-366.

17. Rode AB, Endoh T, Sugimoto N. Tuning riboswitch-mediated gene regulation by rational control of aptamer ligand binding properties. 2015. Angew Chem Int Ed Engl. 54:905-959.

18. Gu H, Furukawa K, Breaker RR. Engineered allosteric ribozymes that sense the bacterial second messenger cyclic diguanosyl 5'-monophosphate. 2012. Anal Chem. 84:4935-4941.

19. Berens C, Suess B. Riboswitch engineering - making the all-important second and third steps. 2015. Curr Opin Biotechnol. 31:10-15.

20. Winkler WC, Nahvi A, Roth A, Collins JA, Breaker RR. Control of gene expression by a natural metabolite-responsive ribozyme. 2004. Nature. 2004. 428:281-286.

21. Lee ER, Baker JL, Weinberg Z, Sudarsan N, Breaker RR. An allosteric self-splicing ribozyme triggered by a bacterial second messenger. 2010. Science. 329:845-848.

22. Serganov A, Patel DJ. Ribozymes, riboswitches and beyond: regulation of gene expression without proteins. 2007. Nat Rev Genet. 8:776-790.

23. Li S, Breaker RR. Eukaryotic TPP riboswitch regulation of alternative splicing involving long-distance base pairing. 2013. Nucleic Acids Res. 41:3022-3031.

24. DebRoy S, Gebbie M, Ramesh A, Goodson JR, Cruz MR, van Hoof A, Winkler WC, Garsin DA. Riboswitches. A riboswitch-containing sRNA controls gene expression by sequestration of a response regulator. 2014. Science. 345:937-940.

25. Mellin JR, Koutero M, Dar D, Nahori MA, Sorek R, Cossart P. Riboswitches. Sequestration of a two-component response regulator by a riboswitch-regulated noncoding RNA. 2014. Science. 345:940-943.

26. Loh E, Dussurget O, Gripenland J, Vaitkevicius K, Tiensuu T, Mandin P, Repoila F, Buchrieser C, Cossart P, Johansson J. A trans-acting riboswitch controls expression of the virulence regulator PrfA in Listeria monocytogenes. 2009. Cell. 2009 139:770-779.

27. Mellin JR, Tiensuu T, Bécavin C, Gouin E, Johansson J, Cossart P. A riboswitch-regulated antisense RNA in Listeria monocytogenes. 2013. PNAS 110:13132-13137.

28. Kim PB, Nelson JW, Breaker RR. An ancient riboswitch class in bacteria regulates purine biosynthesis and one-carbon metabolism. 2015. Mol Cell. 57:317-328.

29. Furukawa K, Ramesh A, Zhou Z, Weinberg Z, Vallery T, Winkler WC, Breaker RR. Bacterial riboswitches cooperatively bind ni(2+) or co(2+) ions and control expression of heavy metal transporters. 2015. Mol Cell. 57:1088-1098.

30. Baker JL, Sudarsan N, Weinberg Z, Roth A, Stockbridge RB, Breaker RR. Widespread genetic switches and toxicity resistance proteins for fluoride. 2012. Science. 335:233-235.

31. Lundrigan MD, Köster W, Kadner RJ. Transcribed sequences of the Escherichia coli btuB gene control its expression and regulation by vitamin B12. 1991. PNAS. 88:1479-1483.

32. Winkler WC, Cohen-Chalamish S, Breaker RR. An mRNA structure that controls gene expression by binding FMN. 2002. PNAS. 99:15908-15913.

33. Rodionov DA, Vitreschak AG, Mironov AA, Gelfand MS. Regulation of lysine biosynthesis and transport genes in bacteria: yet another RNA riboswitch? 2003. Nucleic Acids Res. 31:6748-6757.

34. Mandal M, Lee M, Barrick JE, Weinberg Z, Emilsson GM, Ruzzo WL, Breaker RR. A glycine-dependent riboswitch that uses cooperative binding to control gene expression. 2004. Science. 306:275-279.

35. Sudarsan N, Lee ER, Weinberg Z, Moy RH, Kim JN, Link KH, Breaker RR. Riboswitches in eubacteria sense the second messenger cyclic di-GMP. 2008. Science. 321:411-413.

36. Price IR, Gaballa A, Ding F, Helmann JD, Ke A. Mn(2+)-Sensing Mechanisms of yybP-ykoY Orphan Riboswitches. 2015. Mol Cell. 57:1110-1123.

37. Barrick JE. Predicting riboswitch regulation on a genomic scale. 2009. Methods Mol Biol. 540:1-13.

38. Breaker RR, Prospects for Riboswitch Discovery and Analysis. 2011. Molecular Cell. 43:867–879.

39. Groher F, Suess B. Synthetic riboswitches - A tool comes of age. 2014. Biochim Biophys Acta. 1839:964-973.

40. Peralta-Yahya, P. P., Zhang, F., del Cardayre, S. B. & Keasling, J. D. Microbial engineering for the production of advanced biofuels. 2012. Nature 488, 320–328.

41. Paddon CJ, Westfall PJ, Pitera DJ, Benjamin K, Fisher K, McPhee D, Leavell MD, Tai A, Main A, Eng D, Polichuk DR, Teoh KH, Reed DW, Treynor T, Lenihan J, Fleck M, Bajad S, Dang G, Dengrove D, Diola D, Dorin G, Ellens KW, Fickes S, Galazzo J, Gaucher SP, Geistlinger T, Henry R, Hepp M, Horning T, Iqbal T, Jiang H, Kizer L, Lieu B, Melis D, Moss N, Regentin R, Secrest S, Tsuruta H, Vazquez R, Westblade LF, Xu L, Yu M, Zhang Y, Zhao L, Lievense J, Covello PS, Keasling JD, Reiling KK, Renninger NS, and Newman JD High-level semi-synthetic production of the potent antimalarial artemisinin. 2013. Nature 496, 528–532.

42. Kemmer C, Gitzinger M, Daoud-El Baba M, Djonov V, Stelling J and Fussenegger M. Self-sufficient control of urate homeostasis in mice by a synthetic circuit. 2010. Nature Biotechnol. 28, 355–360.

43. Rössger, K., Charpin-El-Hamri, G. & Fussenegger, M. A closed-loop synthetic gene circuit for the treatment of diet-induced obesity in mice. 2013. Nature Commun. 4:2825.

44. Ausländer D, Ausländer S, Charpin-El Hamri G, Sedlmayer F, Müller M, Frey O, Hierlemann A, Stelling J, and Fussenegger M. A synthetic multifunctional mammalian pH sensor and CO2 transgene-control device.2014. Mol. Cell 55, 397–408.

45. Goodson MS, Harbaugh SV, Chushak YG, Kelley-Loughnane N. Integrating and amplifying signal from riboswitch biosensors. 2015. Methods Enzymol. 550:73-91.

46. P.E.M. Purnick PEM, R. Weiss. The second wave of synthetic biology: from modules to systems. 2009. Nat. Rev. Mol. Cell Biol. 10:410–422.

47. Khalil AS and Collins JJ. Synthetic biology: applications come of age. 2010. Nat. Rev. Genet. 11:367–379.

48. Callura JM, Cantor CR, and Collins JJ. Genetic switchboard for synthetic biology applications. 2012. PNAS. 109:5850–5855

49. Mutalik VK, Qi L, Guimaraes JC, Lucks JB, and Arkin AP. Rationally designed families of orthogonal RNA regulators of translation. 2012. Nat. Chem. Biol. 8:447–454.

50. Rodrigo G, Landrain TE, Jaramillo A. De novo automated design of small RNA circuits for engineering synthetic riboregulation in living cells. 2012. PNAS 109:15271–15276.

51. Win MN and Smolke CD Higher-order cellular information processing with synthetic RNA devices. 2008. Science, 322:456–460.

52. Salis H, Tamsir A, and Voigt C. 2009. Engineering bacterial signals and sensors. Contrib Microbiol. 16:194-225.

53. Weigand JE, Sanchez M, Gunnesch EB, Zeiher S, Schroeder R, Suess B. Screening for engineered neomycin riboswitches that control translation initiation.2008. RNA. 14:89-97.

54. Colas P. Combinatorial protein reagents to manipulate protein function. 2000. Curr Opin Chem Biol. 4:54-59.

55. Ellington AD, Szostak JW. In vitro selection of RNA molecules that bind specific ligands. 1990. Nature. 346:818-822.

56. Famulok M, Mayer G. Aptamers and SELEX in Chemistry & Biology. 2014. Chem Biol. 21:1055-1058.

57. Xiang D, Shigdar S, Qiao G, Wang T, Kouzani AZ, Zhou SF, Kong L, Li Y, Pu C, and Duan W. Nucleic acid aptamer-guided cancer therapeutics and diagnostics: the next generation of cancer medicine. 2015. Theranostics. 5:23-42.

58. Borujeni A E, Mischler D M, Wang J, Huso W, Salis H M. Automated physics-based design of synthetic riboswitches from diverse aptamers (Manuscript Submitted)

59. Salis HM. The ribosome binding site calculator. 2011. Synthetic Biology. Pt B 498:19-42.

60. Salis HM, Mirsky EA, Voigt CA. Automated design of synthetic ribosome binding sites to control protein expression. 2009. Nat Biotechnol. 27:946-950.

61. Espah Borujeni A1, Channarasappa AS, Salis HM. Translation rate is controlled by coupled trade-offs between site accessibility, selective RNA unfolding and sliding at upstream standby sites. 2014. Nucl Acids Res. 42:2646-2459.

62. Beisel CL, Smolke CD. Design principles for riboswitch function. 2009. PLoS Comput Biol. 5:e1000363.

63. Mathews DH, Sabina J, Zuker M, Turner DH. Expanded sequence dependence of thermodynamic parameters improves prediction of RNA secondary structure. 1999. J Mol Biol. 288:911-940.

64. Cao S, Chen SJ. Predicting structures and stabilities for H-type pseudoknots with interhelix loops. 2009. RNA. 5:696-706.

65. Sperschneider J, Datta A. DotKnot: pseudoknot prediction using the probability dot plot under a refined energy model. 2010. Nucleic Acids Res. 38:e103.

66. Cruz-Toledo J1, McKeague M, Zhang X, Giamberardino A, McConnell E, Francis T, DeRosa MC, Dumontier M. Aptamer Base: a collaborative knowledge base to describe aptamers and SELEX experiments. 2012. Database (Oxford). 2012:bas006.

67. Klusman S. The aptamer handbook: functional oligonucleotides and their applications. (John Wiley and Sons, 2006).

68. Ehrentreich-Förster E, Orgel D, Krause-Griep A, Cech B, Erdmann VA, Bier F, Scheller FW, Rimmele M. Biosensor-based on-site explosives detection using aptamers as recognition elements. 2008. Anal Bioanal Chem. 391:1793-1800.

69. Apodaca DC, Pernites RB, Del Mundo FR, Advincula RC. Detection of 2,4-dinitrotoluene (DNT) as a model system for nitroaromatic compounds via molecularly imprinted short-alkyl-chain SAMs. 2011. Langmuir. 27:6768-6779.

70. Styles JA, Cross MF. Activity of 2,4,6-trinitrotoluene in an in vitro mammalian gene mutation assay. 1983. Cancer Lett. 20:103-108.

71. Levine BS, Furedi EM, Gordon DE, Barkley JJ, Lish PM. Toxic interactions of the munitions compounds TNT and RDX in F344 rats. 1990. Fundam Appl Toxicol. 15:373-380.

72. Davidson ME, Harbaugh SV, Chushak YG, Stone MO, Kelley-Loughnane N. Development of a 2,4-dinitrotoluene-responsive synthetic riboswitch in E. coli cells. 2013. ACS Chem Biol. 8:234-241.

ACADEMIC VITA

Walker Huso
wdh126@psu.edu

Academics

Pennsylvania State University

Schreyer Honors College

Dean's List: 2011-2015

Honors and Awards

Schreyer Honors Scholar (Four Year Academic Scholarship)

Penn State York Honors Award

President's Freshman Award

George H. Deike Scholarship

R. Swenson Scholarship

Klingler Chemical Engineer Scholarship

Rayfield Honors Scholarship

College of Engineering Excellence Scholarship

Professional Experience

Pennsylvania State University : Honors Thesis Research –2013-2015

Rapid automated optimization of riboswitch function for synthetic biology

Advisor: Dr. Howard Salis, Department of Chemical and Biological Engineering

Pennsylvania State University: Research Publication 2015

Borujeni AE, Mishler DM, Wang J, Huso W, and Salis HM. Automated Physics-based Design of Synthetic Riboswitches from Diverse Aptamers. (Manuscript submitted)

Johns Hopkins School of Medicine Brain Science Institute: Summer 2010–2014

Research Assistant on drug discovery team. Screened libraries of compounds using high throughput assays; Expression and purification of recombinant enzyme; HPLC, and cell culture.

Accent Interactive — Summer 2009.

Developed client websites using HTML, CSS, and JavaScript. Assisted with client photo shoots, still photography, and videography.

Computational and Laboratory Skills

Python, C++, MatLab, Mathmatica, SolidWorks, NCBI tools, HYSYS

Presentations

2011: “Glutaminase Inhibitors” Brain Science Inst. Student

2012: “Expression of Recombinant Glutaminase” Brain Science Inst. Student

2013: “FPLC Purification of DAA-Oxidase” Brain Science Inst. Student

2014: “High Throughput Screening for xCT Inhibitors” Brain Science Inst. Student

Memberships

Tau Beta Pi Engineering Honors Society (invited as a junior)

Golden Key Honors Society 2014

Activities

Tutor — Fall 2012 Penn Sate Faculty recommended tutor in Organic Chemistry.

Habitat for Humanity Volunteer — Team rebuilt 7 houses in past 6 summers in Baltimore.

Penn State Rifle Club — 2013. Secretary of Penn State Rifle Club; Olympic style competitive team.